LM-03K021
April 5, 2003

The Stress Corrosion Crack Growth Rate of Alloy 600 Heat Affected Zones Exposed to High Purity Water

George A. Young & Nathan Lewis

NOTICE

The Stress Corrosion Crack Growth Rate of Alloy 600 Heat Affected Zones Exposed to High Purity Water

George A. Young and Nathan Lewis
Lockheed Martin Corporation
Schenectady, NY 12301-1072

Abstract

Grain boundary chromium carbides improve the resistance of nickel based alloys to primary water stress corrosion cracking (PWSCC). However, in weld heat affected zones (HAZ's), thermal cycles from fusion welding can solutionize beneficial grain boundary carbides, produce locally high residual stresses and strains, and promote PWSCC. The present research investigates the crack growth rate of an A600 HAZ as a function of test temperature. The A600 HAZ was fabricated by building up a gas-tungsten-arc-weld deposit of EN82H filler metal onto a mill-annealed A600 plate. Fracture mechanics based, stress corrosion crack growth rate testing was performed in high purity water between 600°F and 680°F at an initial stress intensity factor of 40 ksi$\sqrt{in}$ and at a constant electrochemical potential. The HAZ samples exhibited significant SCC, entirely within the HAZ at all temperatures tested. While the HAZ samples showed the same temperature dependence for SCC as the base material (HAZ: $29.8 \pm 11.2|_{95\%}$ kcal/mol vs. A600 Base: $35.3 \pm 2.58|_{95\%}$ kcal/mol), the crack growth rates were ~30X faster than the A600 base material tested at the same conditions. The increased crack growth rates of the HAZ is attributed to fewer intergranular chromium rich carbides and to increased plastic strain in the HAZ as compared to the unaffected base material.

Background

Nickel-chromium-iron alloys such as Alloy 600 (A600) and Alloy 690 (A690) are often used in nuclear environments due to their resistance to general corrosion, localized corrosion, and to stress corrosion cracking (SCC). When used in deaerated primary water environments, A600 and A690 are heat treated to precipitate chromium rich carbides on the grain boundaries to maximize the resistance of these alloys to primary water stress corrosion cracking (PWSCC). In A600, the carbide can be Cr_7C_3 or $Cr_{23}C_6$, while in A690, the $Cr_{23}C_6$ precipitate is the most common. However, fusion welding can solutionize grain boundary carbides and produce increased residual tensile stresses in the HAZ [1] that may render the heat affected zone (HAZ) more susceptible to primary water stress corrosion cracking (PWSCC) than the unaffected base metal.

Primary water SCC has been reported in A600 control rod drive mechanism (CRDM) head penetrations near the A600 / E-182 weld interface (*i.e.* near the HAZ) [2-4]. Most recently, PWSCC in the CRDM of an A600 nozzle has been implicated in the Davis-Besse reactor vessel head leaking [5]. In the CRDM cracking, an as welded, partial penetration shielded-manual-arc-weld may solutionize intergranular chromium carbides adjacent to the weld deposit [2] and contributes to locally high plastic strains and residual tensile stresses on the order of 100 ksi [1].

In spite of concerns with HAZ SCC, limited data exist for the crack growth rates of heat affected zones. In part, this is due to the small scale of material affected, typically on the order of ~1 mm in width for gas-tungsten-arc-welding (GTAW). Furthermore, a HAZ is not uniform in its structure or composition. Near the fusion zone, welding temperatures can solutionize precipitates, cause local melting via constitutional liquation, and promote diffusional segregation of alloying elements or environmental contaminants (*e.g.* hydrogen). Similarly, thermal cycles from multi-pass welds or from post-weld heat treatments may cause precipitation or elemental segregation to grain boundaries.

Given the complex thermal history of a multi-pass weldment, fabrication of a bulk HAZ sample (typically via Gleeble methods) is a difficult task. The distance away from the fusion zone that is of interest must be defined, since this will dictate the relevant thermal cycles. Once the distance from the fusion zone is selected, parameters that must be defined include: (1) the peak temperature, (2) the hold time at the peak temperature, (3) the appropriate mechanical conditions during thermal cycles, (4) the cooling rate, (5) the thermo-mechanical effects of subsequent weld beads and (6) the appropriate post weld heat treatment. Since there is no *a priori* way of determining the precise distance away from the fusion zone that is most susceptible to SCC, testing of simulated HAZ's likely involves multiple samples with a range of thermal histories.

Instead of testing a simulated HAZ, the present testing elected to test samples machined from an actual weldment. The challenge of this method is to (1) precisely machine the notch of the compact tension specimen in the HAZ and (2) to ensure that the fatigue precrack remains in the HAZ. Once the end of the fatigue precrack is in the HAZ, it is believed that SCC will seek the most susceptible path in terms of microstructure, microchemistry, and residual stresses and strains. In this manner, reliable data can be obtained to characterize the growth rate of PWSCC in HAZ's [6, 7].

Experimental Procedure

Materials

The compositions of the A600 and EN82H weld wire used in this study are given in Table 1. The HAZ specimens were machined from the interface between the 3" thick A600 plate and a 3" thick multi-pass, automatic gas-tungsten-arc-weld (GTAW). The GTAW was deposited with the parameters given in Table 2. The weld deposit was approximately 3" high x 3.25" wide x 15" long while the base plate was nominally 3" thick x 12" wide x 24" long. No post weld heat treatment was employed.

Table 1. *Chemical Compositions of Alloy 600 and EN82H Filler Metal*

Alloy	Heat	Ni	Cr	Fe	C	Mn	Si	Cu	Nb+Ta	Ti
A600	44639	76.37	14.74	7.35	0.071	0.350	0.31	0.020	---	---
EN82H	YM7553	71.5	20.1	2.39	0.04	2.88	0.08	0.01	2.3	0.47

Table 2. *Summary of Welding Parameters Used to Make the EN82H Weld Deposit*

Filler Metal	Polarity	Shielding Gas	Current (Amps)	Voltage (Volts)	Travel Speed (in./min.)	Wire Feed (in./min.)
0.045" dia. EN82H	DCSP	95%Ar/5%H_2	310	12.5	6.5	180

Stress Corrosion Testing

Compact tension (CT) specimens (1.0T) were machined from the base material and the heat affected zone in the S-L orientation. In the HAZ samples, the notch root of the CT specimen was in the HAZ as shown schematically in Figure 1. In order to facilitate precise location of the notch, oversized machining blanks were polished and etched prior to machining. After machining, the specimens were fatigue precracked approximately 100 mils beyond the machined notch and tested in hydrogen deaerated water under constant load to determine their SCC growth rate. The nominal conditions of the SCC testing are given in Table 3. The dissolved hydrogen concentrations were chosen to be at an approximately constant electrochemical potential (~0 to +10mV) relative to the Ni/NiO phase stability line. Additional details of the Ni/NiO phase stability can be found in References [8, 9].

Table 3. *Parameters Used in the High Purity Water Stress Corrosion Tests*

Temperature (°F / °C)	Hydrogen (scc/kg)	ΔECP from Ni/NiO (mV)	Initial Stress Intensity Factor (ksi $\sqrt{in}$)
600 / 316	9	0 to +10	40
640 / 338	18	0 to +10	40
680 / 360	30	0 to +10	40

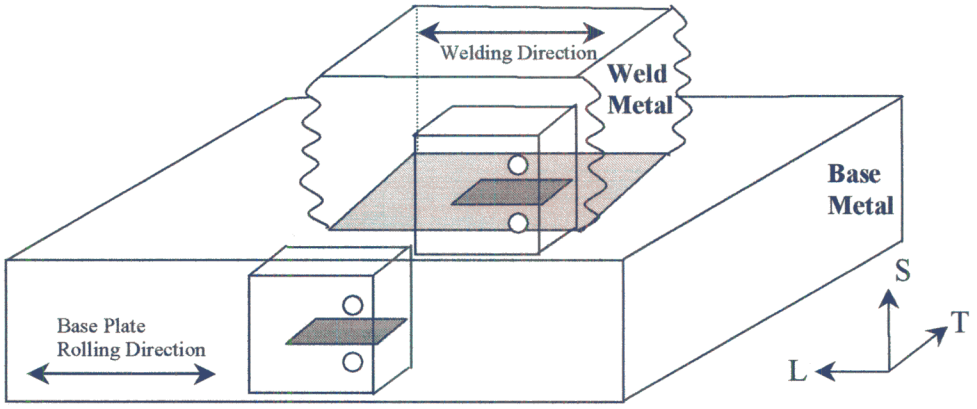

Figure 1. *Schematic of the HAZ specimen and base metal specimen orientation relative to the weld deposit. For the HAZ specimens, the notch tip lies in the HAZ. The sketch is not to scale.*

Results and Discussion

Specimen Fabrication

For the HAZ samples, post-test inspection revealed that all of the machined notches, fatigue precracks, and subsequent SCC were located within the HAZ. The location of a typical notch and precrack is shown in Figure 2. For some specimens, the notch and precrack were located closer to the EN82H weld metal. As will be shown below, it appears that in the weld investigated, the preferred SCC plane is approximately 20 mils (~0.5 mm) from the EN82H / A600 interface.

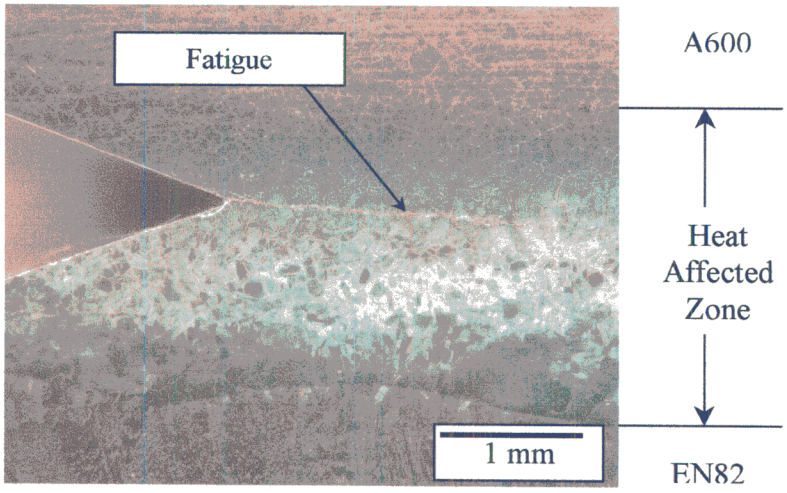

Figure 2. *Light macrograph of the CT specimen notch and fatigue precrack. Note that the precrack is entirely within the A600 HAZ. 8:1 Phosphoric Acid, Electrolytic Etch.*

A600 Base and A600 HAZ Crack Growth Rates

In-situ instrumentation of the crack mouth opening displacement was conducted with linear variable displacement transducers (LVDT's). The LVDT instrumentation was used to define the start of crack growth. However, instrumentation was not used to determine the crack growth rates. Since out of plane cracking and extensive crack branching were observed with the HAZ samples (and likely bias the instrumentation) crack growth rates were calculated from visual measurements of the crack lengths. To facilitate crack measurement, the samples were heat tinted prior to measurement and thirty separate measurements across the CT specimen width were used to determine the average and maximum crack lengths. The SCC test results are summarized in Figure 3 and show that the crack growth rates for HAZ samples range between ~0.5 mils/day at 600°F to ~3.6 mils/day at 680°F. Relative to the A600 base plate (green squares) the HAZ samples (blue circles) crack approximately 30X faster.

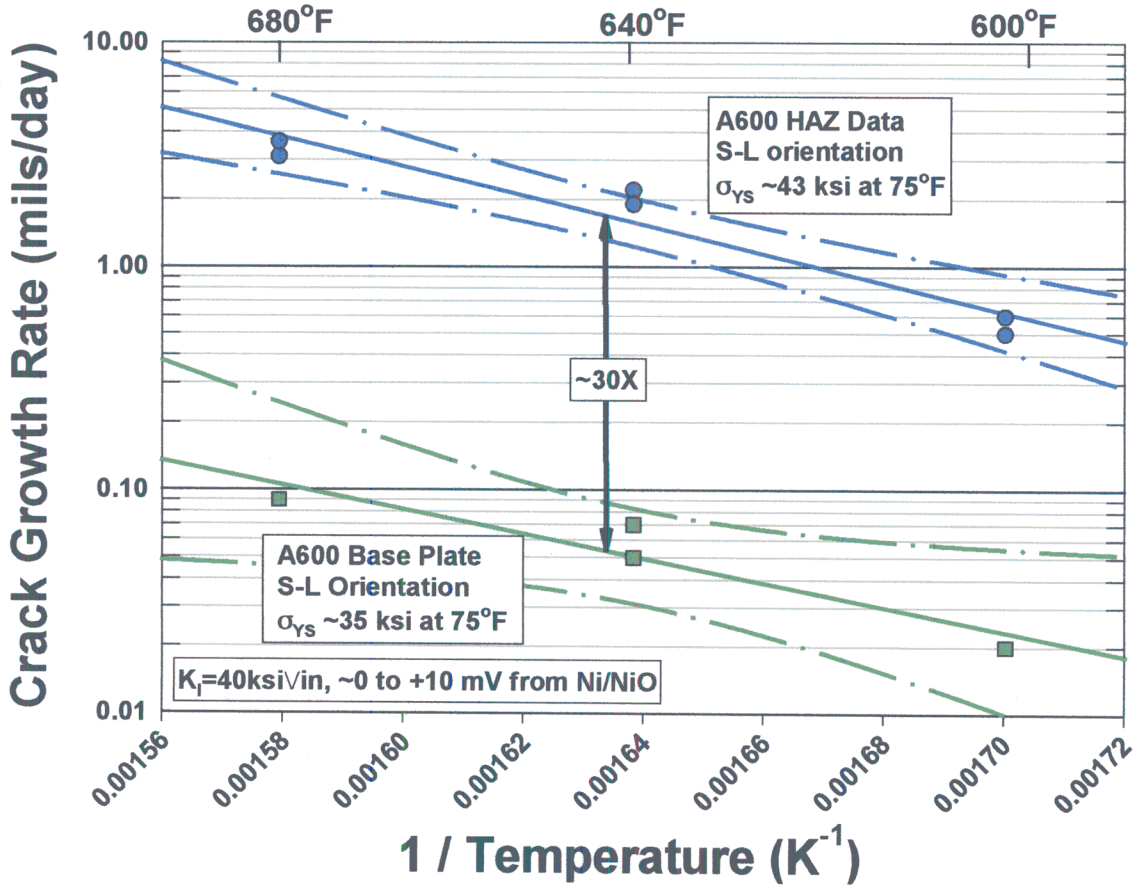

Figure 3. *Comparison of the A600 HAZ data (blue points) with a prediction for typical high temperature annealed A600 (i.e. the unaffected base material).*

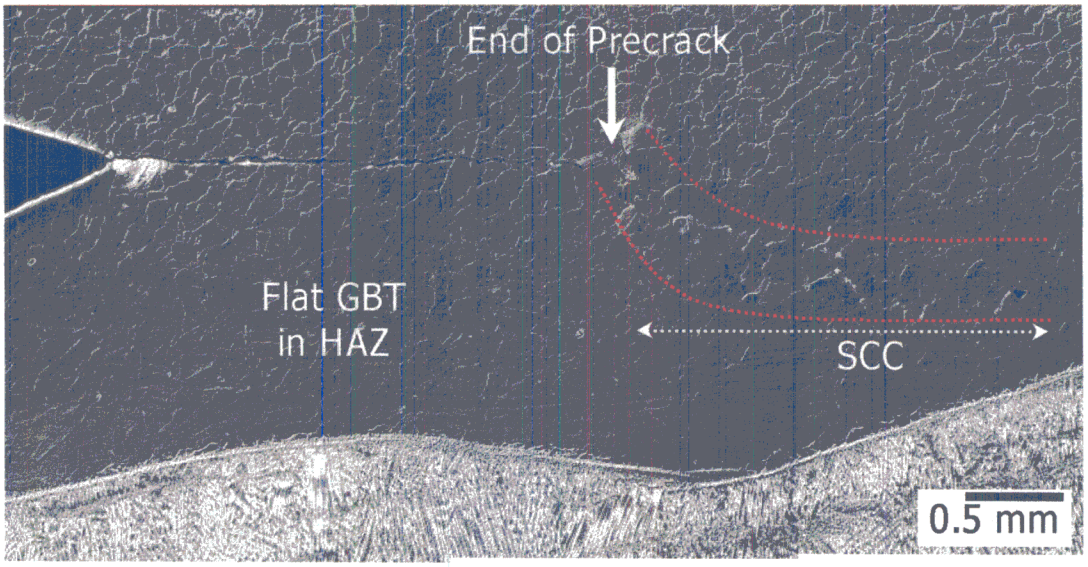

Figure 4. *Cross section of the fatigue precrack and SCC crack plane from sample HB2-12 tested at 680°F. GBT refers to the grain boundary topography.*

Activation Energy Analysis

Primary water stress corrosion cracking often follows Arrhenius-type temperature dependence. The slope of the trend line in Figure 3 is proportional to the apparent activation energy for crack growth. Table 4 summarizes the apparent activation energy ($Q_{Apparent}$) along with the pre-exponential factor (A_0) for both corrected average crack growth rate of the HAZ material. The corrected average crack growth rate exhibits an activation energy of ~29.8 kcal/mol (~125 kJ/mol). The A600 HAZ activation energy is well within the 95% confidence interval of the apparent activation energy for SCC of A600 base metal in the high temperature annealed condition as shown in Figure 5. Note that the HAZ data are not compared to the apparent activation energy for the A600 base metal tested in the present study. While the slope of the A600 base metal data is similar to the HAZ data (Figure 3), the sparse A600 data in the current testing make the bounds on the apparent activation energy quite large. The activation energy of 35.3 kcal/mol is from a much larger dataset.

Table 4. ***Summary of Apparent Activation Energies:*** $\dot{a} = A_0 \exp\left(-Q_{Apparent} / RT\right)$

Process	Pre-exponential, A_0 (mils/day)	A_0 95% Confidence (mils/day)	Apparent Activation Energy, $Q_{Apparent}$ (kcal/mol) / (kJ/mol)	$Q_{Apparent}$ 95% Confidence (kcal/mol) / (kJ/mol)	R^2
HAZ	7.40×10^{10}	7.03×10^{6} – 7.79×10^{14}	29.8 / 125	±11.2 / ±47.0	0.93148
HTA* A600 Base Material	---	---	35.3 / 148	±2.58 / ±10.8	---

*"HTA" = high temperature annealed

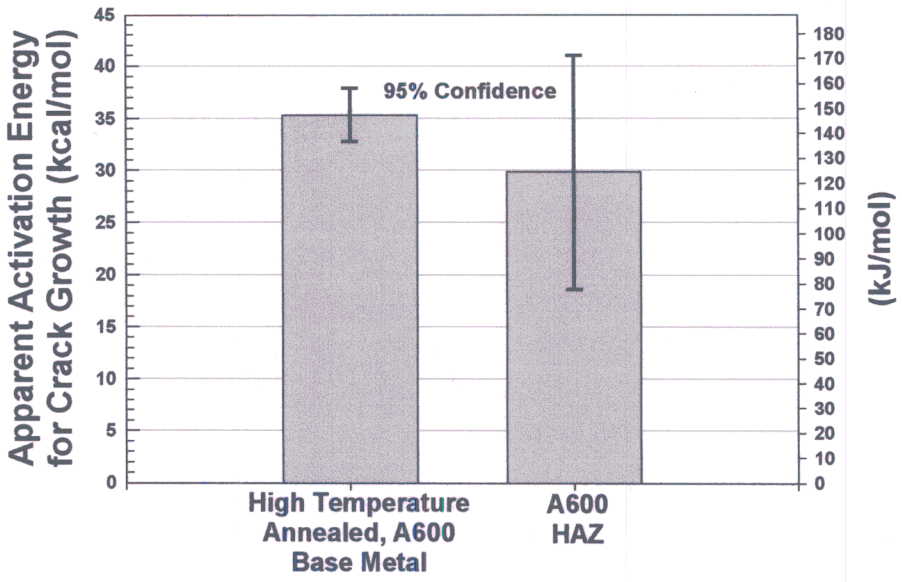

Figure 5. *Comparison of the apparent activation energies for primary water SCC between the 2002 Engineering Model for A600 (left) and the A600 HAZ data (right). The A600 base metal Q is well within the 95% confidence interval of the HAZ data.*

HAZ Microstructure

A typical HAZ microstructure is shown in Figure 6 where the edge of the EN82H weld is on the right and unaffected base metal is toward the left. When view with Nomarski differential interference contrast illumination, the grain boundary topography is flat, indicative of little intergranular chromium carbide precipitation. Near the SCC crack, the ASTM grain size is approximately 3.6 or ~100 μm diameter grains. While extensive secondary cracking was observed in the HAZ, no cracking was observed in either the unaffected base metal or in the EN82H weld metal.

The HAZ region was also investigated via transmission electron microscopy (TEM), as shown in Figures 7, 8, and 9. In Figure 7, TEM shows that there are fine, discontinuos $M_{23}C_6$-type carbides on many of the HAZ grain boundaries. In contrast, the unaffected A600 base metal shows extensive inter- and intra-granular M_7C_3-type carbide precipitation. One likely scenario is that the first welding pass solutionized the M_7C_3 carbides while subsequent welding passes acted to precipitate the $M_{23}C_6$ carbides.

HAZ Microchemistry

Compositional profiles of unaffected base metal and HAZ grain boundaries show the effect of the difference in chromium carbide structure on the near grain boundary composition (Figure 8.). The HAZ shows a much narrower Cr depleted zone, consistent with the fewer, finer $Cr_{23}C_6$-type carbides relative to the extensive Cr_7C_3 carbide precipitation in the base metal. The near grain boundary chromium concentration is likely important to crack tip corrosion processes and to the fugacity of hydrogen produced via corrosion. For example, the higher average chromium concentration near the HAZ grain boundaries likely increases the fugacity of hydrogen produced during the corrosion reaction $A600 + H_2O(l) \rightarrow (Ni, Cr, Fe)O(s) + H_2(g)$, where Cr can substitute into the NiO-type oxide. The types of crack tip oxides and the resultant hydrogen fugacities are discussed elsewhere [10].

HAZ Deformation

In addition to the difference in carbide structure, TEM examination also showed that the HAZ contained significantly more plastic strain than the unaffected base metal. Figure 9 shows TEM micrographs between the HAZ (left) and the base metal (right). The HAZ micrographs show both increased dislocation density and the accumulation of low angle boundaries relative to the unaffected A600 base material. Plastic strains in the HAZ were further characterized via microhardness and electron backscatter diffraction. A microhardness traverse (Figure 10) shows that the hardness trend is EN82H (KHN=255) > A600 HAZ (KHN=242) > A600 Base Metal (KHN=228).

Figure 11 shows a map of the intra-grain, plastic strains for the A600 base metal, HAZ, and the EN82H weld adjacent to the HAZ. The base metal shows very low strains (blue) while the HAZ and weld show significant plastic strain (green through red), in agreement with the TEM findings. The increased strain in the HAZ is also consistent with its SCC susceptibility and its higher strength and decreased ductility as discussed below. In Figure 11, the white points are areas where no diffraction pattern could be determined.

The EBSD data can also be used to quantify the amount of residual plastic strain in the HAZ [11-15]. However, strain quantification requires a suitable calibration curve that relates the average intra-grain misorientation or "amis" parameter to the plastic strain. Calibration curves for annealed A600, annealed EN82H weld filler metal, and for high purity nickel are given in Figure 12. The amis parameter measurements for the unaffected base metal, the HAZ, and the EN82H weld metal adjacent to the HAZ are 0.3°, 1.5°, and 1.4° respectively. These amis values correspond to ~0% plastic strain in the base metal, ~6% in the HAZ and ~4% in the weld metal adjacent to the HAZ.

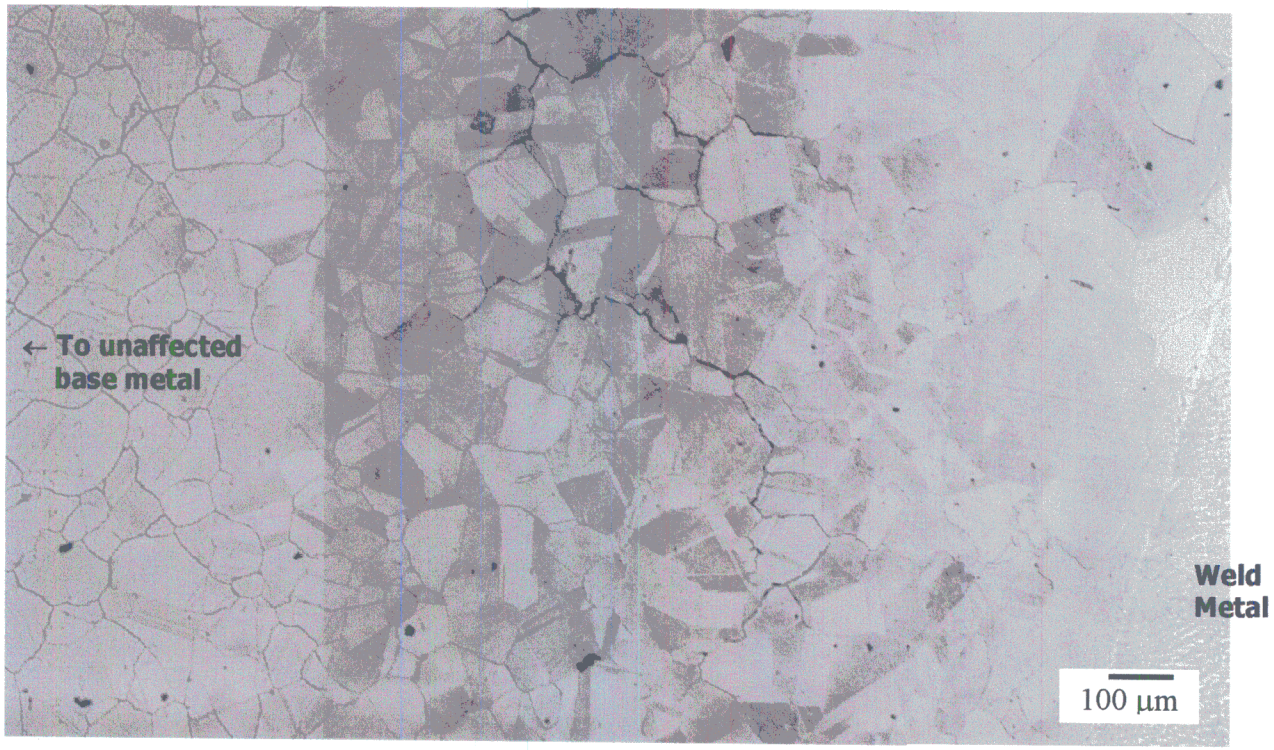

Figure 6. *Light micrograph of a HAZ SCC crack. Note the intergranular crack path and crack branching. 8:1 phosphoric acid, Nomarski, DIC.*

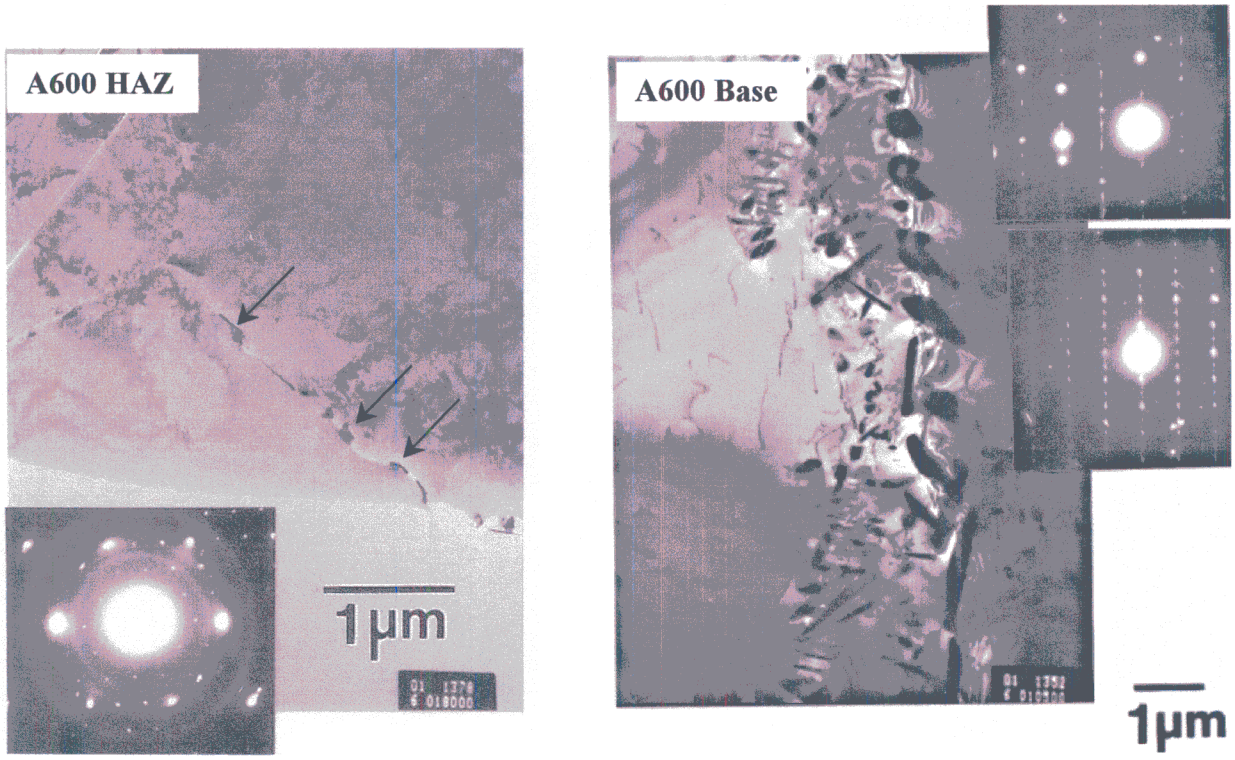

Figure 7. *Transmission electron microscopy of the A600 HAZ (left) and the A600 base material (right). Note the few $M_{23}C_6$-type carbides in the HAZ (arrows) while the unaffected base material displays extensive inter- and intra-granular M_7C_3-type carbides.*

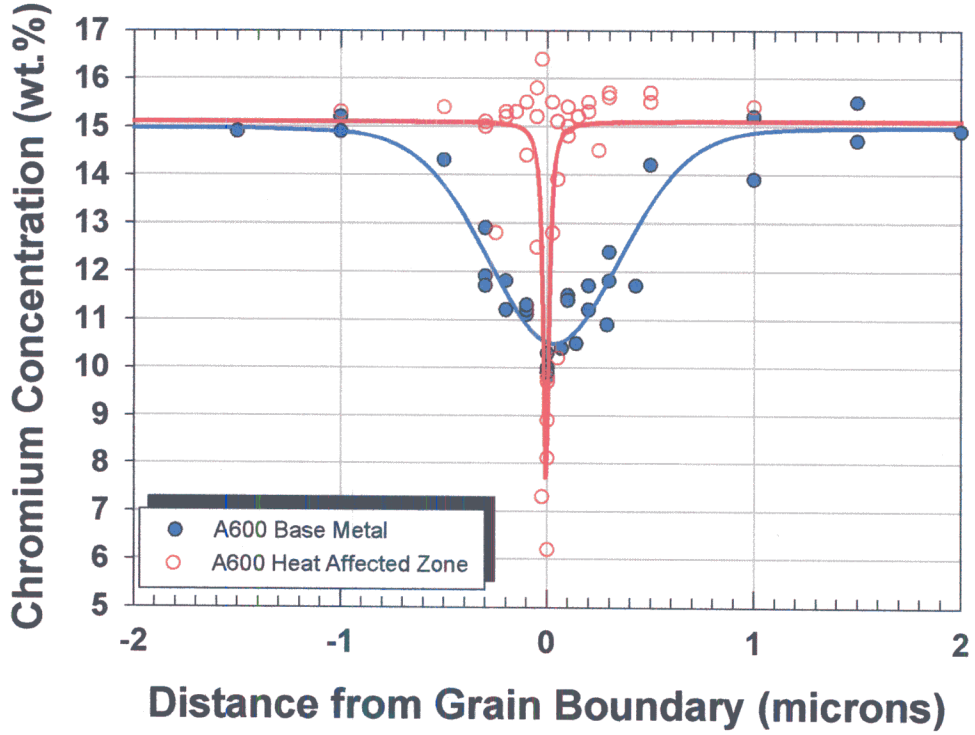

Figure 8. *Comparison of chromium depletion near unaffected base metal (solid blue points) and the heat affected zone (open red points). The HAZ shows a much sharper Cr depleted zone, consistent with the fewer, finer $Cr_{23}C_6$-type carbides relative to the extensive Cr_7C_3 carbide precipitation in the base metal.*

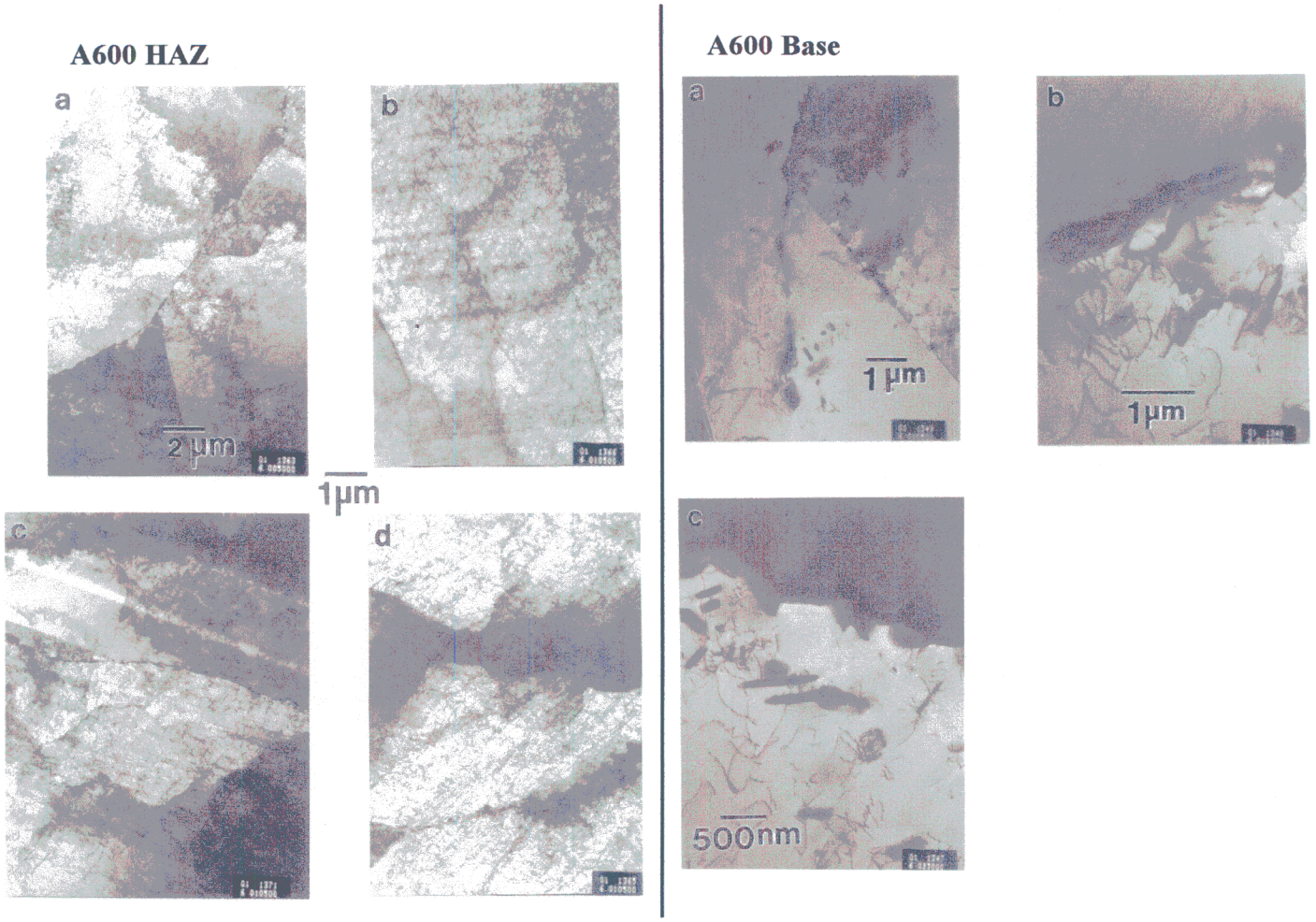

Figure 9. *Transmission electron microscopy of the A600 HAZ (left) and the A600 base material (right). Note the increased dislocation density and the bend contours in the HAZ while the A600 base material is relatively strain free.*

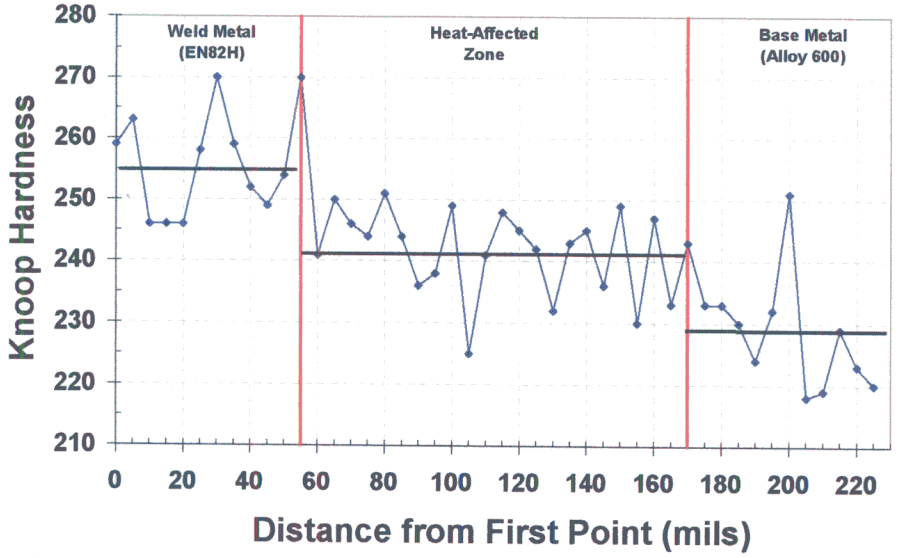

Figure 10. *Microhardness traverse across the EN82H weld, A600 HAZ and A600 base metal. Knoop hardness, 500 gf.*

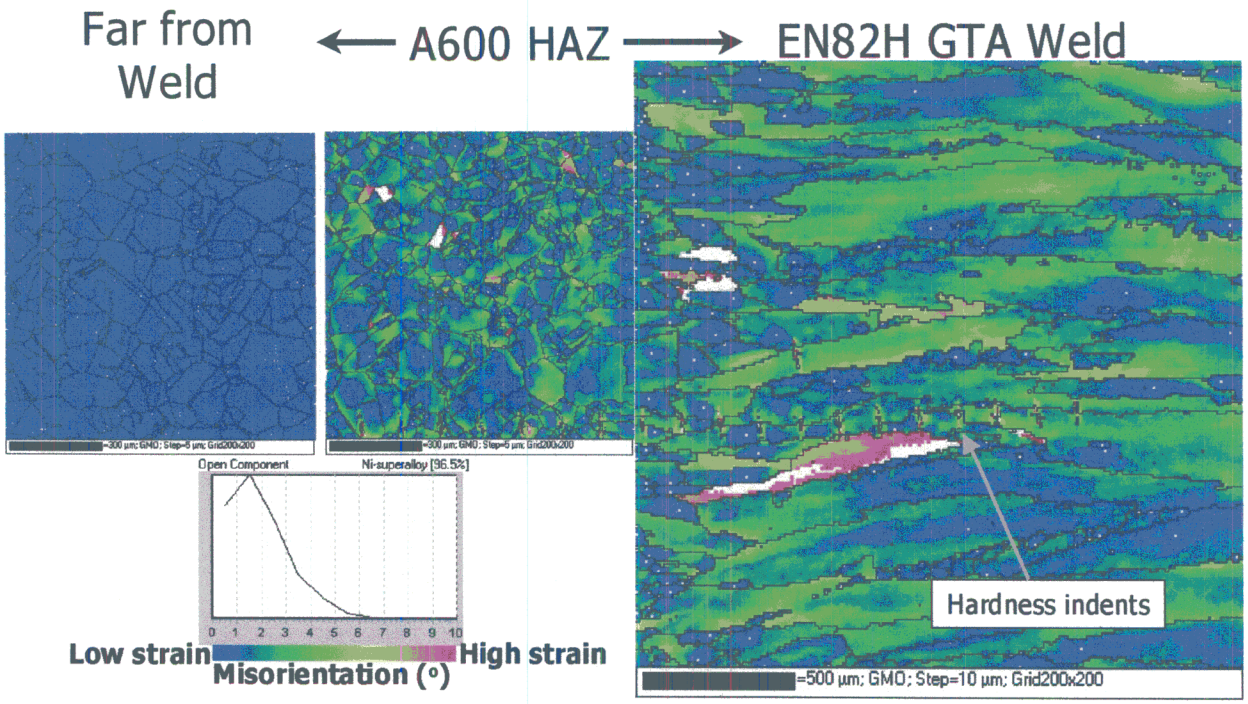

Figure 11. *Electron backscatter diffraction maps of the intra-grain strains. The A600 base metal (left) shows very little strain while the HAZ and the near HAZ weld show significant strains.*

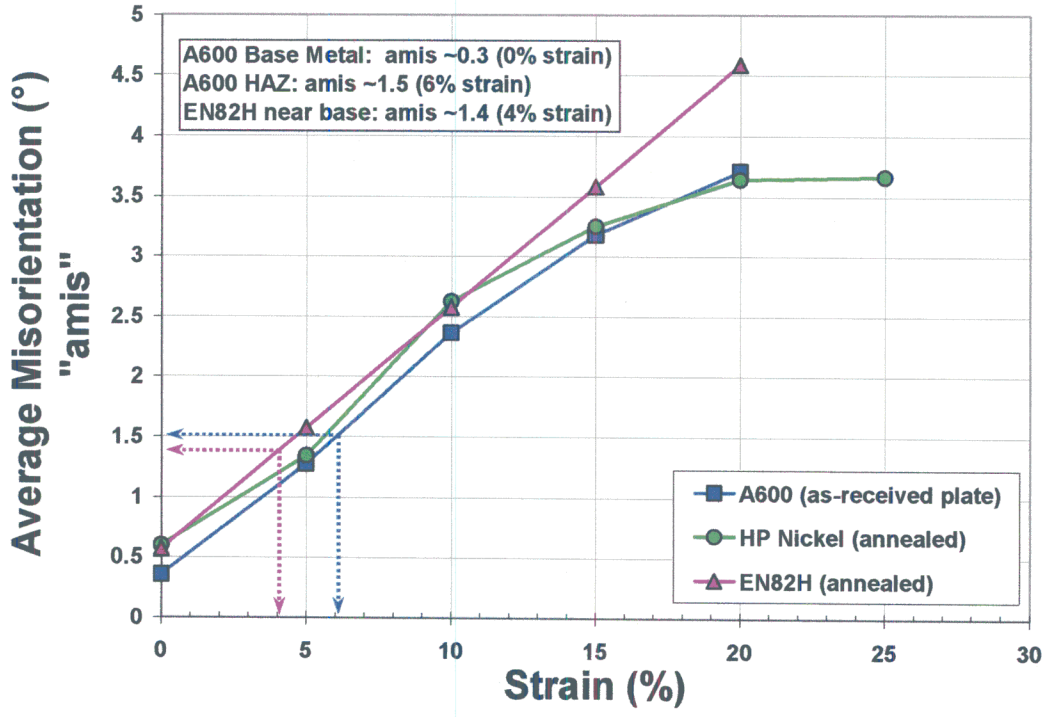

Figure 12. *Calibration curves relating the applied tensile strain at room temperature to the average intra-grain misorientation (amis) parameter. The HAZ samples exhibited ~6% plastic strain.*

Effect of Coolant Hydrogen

For wrought A600 with significant precipitation of intergranular chromium rich carbides (i.e. the A600 base metal), the SCC crack growth rate exhibits a maximum near the Ni/NiO phase transition [8]. The effect of electrochemical potential on the SCCGR is shown schematically in Figure 13. For A600 base metal, the crack growth rate at the Ni/NiO phase transition is approximately 2.8X faster than rates measured far into the nickel metal regime [8]. However, other alloys (X-750 Condition AH and EN82H weld metal) show a larger effect of coolant hydrogen on the SCCGR, on the order of 8X and the maximum crack growth rate is shifted into the NiO stability regime (Figure 13). The A600 HAZ has few intergranular chromium rich carbides compared to typical high temperature annealed A600 material (with extensive intergranular M_7C_3 and or $M_{23}C_6$ precipitation). The magnitude of the effect of electrochemical potential might be greater than the 2.8X observed in the A600 base metal. Additional testing on A600 HAZ's as a function of electrochemical potential relative to the Ni/NiO phase transition is needed before the magnitude of the effect on A600 HAZ's can be determined.

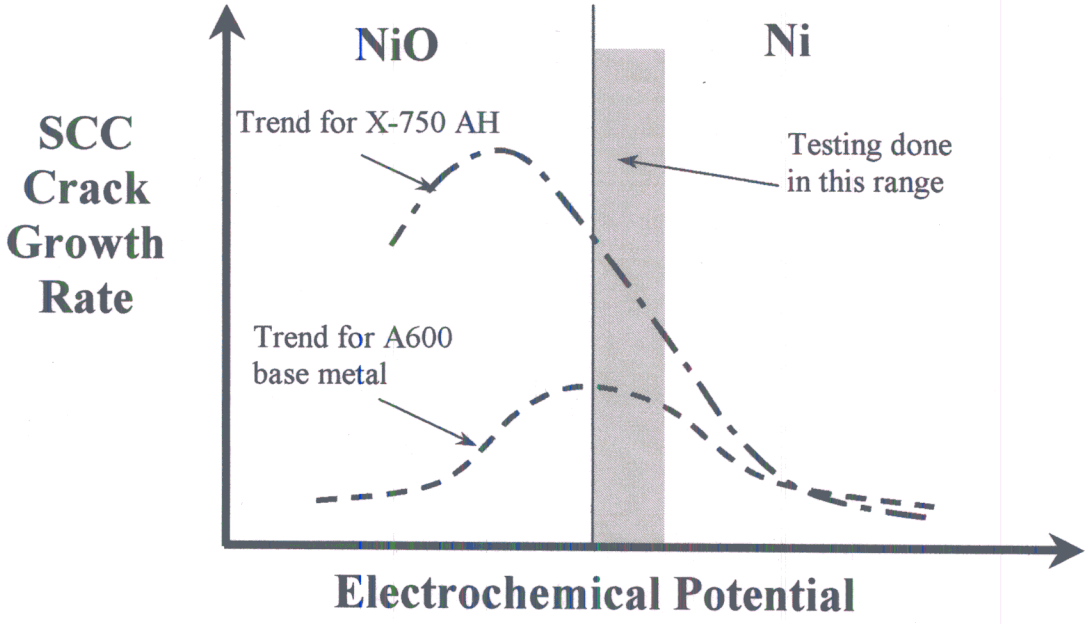

Figure 13. *Schematic illustration of the effect of electrochemical potential on the stress corrosion crack growth rate of nickel-base alloys in high temperature, high purity water. Reference [8] provides quantitative information.*

Conclusions

- Relative to high temperature annealed base material, A600 HAZ's are highly susceptible stress corrosion cracking in high purity, high temperature water. The increased susceptibility of the HAZ is attributed to their microstructure (fewer, finer intergranular chromium carbides) and to increased levels of plastic strain (~6% for the HAZ tested).

- The apparent activation energy for SCCGR of A600 HAZ material in primary water $29.8 \pm 11.2|_{95\%}$ kcal/mol which is within experimental error of the value for the unaffected, A600 base metal ($35.3 \pm 2.58|_{95\%}$ kcal/mol).

- When stress corrosion cracking of A600 heat affected zones is a concern, welding heat input, inter-pass temperatures, and post weld heat treatments should be engineered to promote intergranular chromium carbide precipitation and to minimize residual plastic strains.

Acknowledgements

Dr. Steve Attanasio, Dr. Dave Morton, Mr. John Mullen, Dr. Weldon Wilkening and Mr. John Wuthrich provided critical input to the test procedure and data analysis. Mr. Ron Polsinelli and Mr. Charles Tricou provided helpful comments and fabricated the CT specimens. Ms. Michelle Othon of the General Electric Global Research and Development Center performed the OIM analyses and Dr. Luke Brewer of provided helpful input to the manuscript.

References

1. Hall, J.F., *et al. Measurement of Residual Stresses in Alloy 600 Pressurizer Penetrations*. in *Conference on the Contribution of Materials Investigation to the Resolution of Problems Encountered in Pressurized Water Reactors*. 1994. Paris: Societe Francaise d'Energie Nucleare.
2. Buisine, D., *et al.*, *Stress Corrosion Cracking in the Vessel Closure Head Penetrations of French PWR's*, in *Sixth International Symposium on Environmental Degradation of Materials in Nuclear Power Systems-Water Reactors*, R.E. Gold and E.P. Simonen, Editors. 1993, TMS: San Diego, CA. p. 845-853.
3. NRC, *Circumferential Cracking of Reactor Pressure Vessel Head Penetration Nozzles*, NRC Bulletin, 2002-01, United States Nuclear Regulatory Commission, Washington, D.C., 3 August 2001.
4. Strosnider, J.R., *Staff Preliminary Technical Assessment of Reactor Pressure Vessel Head Penetration Nozzle Cracking*, Preliminary Technical Assessment, Unites States Nuclear Regulatory Commission, Washington, D.C., 4 December 2001.
5. *Davis-Besse Reactor Vessel Head Damage*, NRC Update, U.S. Nuclear Regulatory Commission, November 2002.

6. Andresen, P.L., *et al. Mechanisms and Kinetics of SCC in Stainless Steels*. in *10th International Conference on Environmental Degradation of Materials in Nuclear Power Systems - Water Reactors*. 2001. Lake Tahoe, NV: NACE.
7. Kilian, R., *et al. Intergranular Stress Corrosion Cracking of Stainless Steel Piping Materials in BWR Environments*. in *10th International Conference on Environmental Degradation of Materials in Nuclear Power Systems - Water Reactors*. 2001. Lake Tahoe, NV: NACE.
8. Morton, D.S. *Primary Water SCC Understanding and Characterization Through Fundamental Testing in the Vicinity of the Nickel/Nickel Oxide Phase Transition*. in *10th International Conference on Environmental Degradation of Materials in Nuclear Power Systems - Water Reactors*. 2001. Lake Tahoe, NV: NACE.
9. Attanasio, S.A., *et al. Measurement of the Nickel/Nickel Oxide Phase Transition in High Temperature Hydrogenated Water Using the Contact Electric Resistance Technique*. in *Tenth International Conference on Environmental Degradation of Materials in Nuclear Power Systems - Water Reactors*. 2001. Lake Tahoe, NV: NACE.
10. Lewis, N., *et al. Stress Corrosion Crack Growth Rate Testing and Analytical Electron Microscopy of Alloy 600 as a Function of Pourbaix Space and Microstructure*. in *Chemistry and Electrochemistry of Corrosion and Stress Corrosion Cracking*. 2001. New Orleans, LA: TMS.
11. Young, G.A. *Quantification of Residual Plastic Strains in Nr-Cr-Mn-Nb GTAW Welds via Electron Backscatter Diffraction*. in *Trends in Welding Research*. 2002. Pine Mt., GA: ASM.
12. Young, G.A. *Factors Affecting the Hydrogen Embrittlement Resistance of Ni-Cr-Mn-Nb Welds*. in *Trends in Welding Research*. 2002. Pine Mt., GA: ASM.
13. Sutliff, J.A., Microscopy and Microanalysis Proceedings, 1999: p. 236.
14. Angeliu, T.M. *Microstructural Characterization of L-Grade Stainless Steels Relative to the IGSCC Behavior in BWR Environments*. in *Corrosion 2001*. 2001: NACE.
15. Lehockey, E.M. and A.M. Brennenstuhl. *Characterization of Plastic Strains and Crystallographic Properties Surrounding Defects in Steam Generator Tubes by Orientation Imaging Microscopy*. in *4th CNS International Steam Generator Conference*. 2002. Toronto, Ontario, Canada.